Nanoscale

Quantitative Comparison of Local Field Enhancement from Tip-Apex and Plasmonic Nanofocusing Excitation via Plasmon-Assisted Field Emission Resonances

Journal:	*Nanoscale*
Manuscript ID	NR-ART-10-2024-004262.R1
Article Type:	Paper
Date Submitted by the Author:	25-Jan-2025
Complete List of Authors:	Lin, Chenfang; Hunan University Li, Jie; Hunan University, ; Li, Guoao; Hunan University Luo, Wenjie; Hunan University Liu, Shuyi; Huazhong University of Science and Technology, Wuhan National Laboratory for Optoelectronics Hammud, Adnan; Fritz-Haber-Institut der Max-Planck-Gesellschaft, Department of Inorganic Chemistry Xia, Yang; Hunan University Pan, Anlian; Hunan University Wolf, Martin; Fritz Haber Institute, Dep. of Physical Chemistry; Freie Universität Berlin, Dep. of Physics Müller, Melanie; Fritz Haber Institute of the Max Planck Society, Department of Physical Chemistry Kumagai, Takashi; Institute for Molecular Science, Center for Mesoscopic Sciences

Quantitative Comparison of Local Field Enhancement from Tip-Apex and Plasmonic Nanofocusing Excitation via Plasmon-Assisted Field Emission Resonances

Chenfang Lin[1*], Jie Li[1], Guoao Li[1], Wenjie Luo[1], Shuyi Liu[2], Adnan Hammud[3], Yang Xia[1], Anlian Pan[1,4], Martin Wolf[5], Melanie Müller[5], Takashi Kumagai[6*]

[1]*Key Laboratory for Micro-Nano Physics and Technology of Hunan Province, State Key Laboratory of Chemo/Biosensing and Chemometrics, Hunan Institute of Optoelectronic Integration, College of Materials Science and Engineering, Hunan University, 410082, Changsha, China.*

[2]*Wuhan National Laboratory for Optoelectronics, Huazhong University of Science and Technology, Wuhan, 430074 China*

[3]*Department of Inorganic Chemistry, Fritz Haber Institute of the Max Planck Society, Faradayweg 4-6, 14195 Berlin, Germany*

[4]*School of Physics and Electronics, Hunan Normal University, 410081, Changsha, China*

[5]*Department of Physical Chemistry, Fritz Haber Institute of the Max Planck Society, Faradayweg 4-6, 14195 Berlin, Germany*

[6]*Center for Mesoscopic Sciences, Institute for Molecular Science, 444-8585 Okazaki, Japan*

*Corresponding authors: lincf@hnu.edu.cn; kuma@ims.ac.jp

ABSTRACT

Plasmonic nanofocusing via off-site excitation offers a promising approach to minimize background light scattering and enhance excitation efficiency in tip-enhanced optical spectroscopy. However, a comprehensive understanding of its effectiveness compared to direct tip-apex excitation remains limited. Here we introduce plasmon-assisted field emission resonances as a practicable approach for quantitative evaluation of the local field enhancement in a scanning-tunneling-microscope junction via off-site excitation compared to direct tip-apex excitation. By using single-groove pyramidal tips suitable for multi-wavelength excitations, we find that the near-field intensity is approximately 3.8 and 1.7 times higher for off-site excitation than for direct apex excitation at excitation wavelengths of 780 nm and 633 nm, respectively. These results are further supported by numerical electromagnetic field simulations. Our findings demonstrate the effective implementation of plasmonic nanofocusing in low-temperature scanning tunneling microscopy, paving the way for more precise and background-free tip-enhanced optical spectroscopy at the atomic scale.

1. Introduction

Integrating optical excitation and photon detection into cryogenic ultrahigh-vacuum (UHV) scanning tunneling microscopes (STM) has enabled tip-enhanced optical spectroscopy with exceptional sensitivity and spatial resolution, providing unprecedented opportunities to study light-matter interactions and material properties at the nanoscale and beyond.[1-4] Recent advances include Raman and photoluminescence mapping with sub-molecular resolution[2-4], imaging of photocurrent distributions through molecular orbitals[5], control of single-molecule reactions[6,7], and the investigation of nanoscale heating.[8,9] A significant advancement has been the stable formation of atomic-scale protrusions at the tip apex, creating "picocavities"[10,11] within the STM junction under cryogenic UHV conditions,[4] which play crucial roles in achieving atomic-scale sensitivity and resolution.[12] While the picocavities enable atomic-scale localization of optical fields, the near-field enhancement and spectral distribution are also influenced by the nano- to mesoscale structure of the tip shaft and apex[4,11,13,14] and the excitation schemes.[15,16] In addition to improving control over the atomistic tip structure, optimization of the excitation efficiency of localized surface plasmons (LSPs) in the STM junction and its accurate characterization is highly desired to further advance optical spectroscopy at atomic scales.

An advanced approach for optimizing and controlling the generation of near fields in tip-enhanced optical spectroscopy is an off-site generation of LSPs via excitation of propagating surface plasmon polaritons (SPPs) and their adiabatic compression along the tapered tip shaft, followed by nanofocusing into the tip apex (**Fig. 1a**).[15,17-20] Broadband SPP excitation and nanofocusing have been demonstrated using single grooves,[21] grating couplers,[19,22] or thin films[23] fabricated into/onto the SPM tip shaft, increasing the local field enhancement and far-field to near-field conversion efficiency compared to direct tip-apex illumination.[18,24,25] Furthermore, SPP nanofocusing allows to eliminate the unwanted far-field background

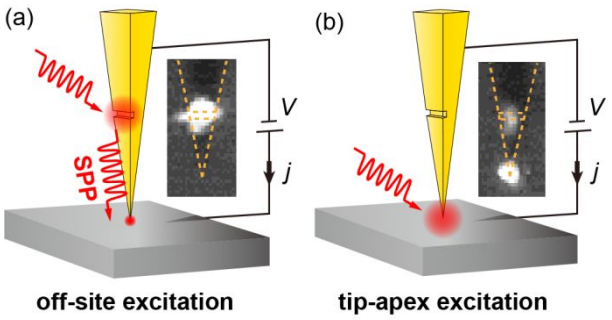

Fig. 1 Schematic off-site (a) and tip-apex (b) excitation. Inset: Optical image of light scattering under groove and apex illumination.

scattering signals in tip-enhanced optical spectroscopy,[16,26-28] and has been employed for nonlinear nano-spectroscopic imaging. [29-31]

While off-site excitation schemes employing SPP nanofocusing have been extensively explored in tip-enhanced optical spectroscopy based on atomic force microscopy under ambient conditions[16,20,21,23,31-36], their application in low-temperature STM for atomic-scale optical spectroscopy, has only recently been initiated[37] and remains underdeveloped. While far-field background is not very critical in tip-enhanced Raman spectroscopy of submonolayer molecules[38] or 2D materials[39,40] on Au or Ag substrates, background scattering becomes a significant problem when conducting tip-enhanced photoluminescence spectroscopy of 2D materials[41] and atomic-scale optical spectroscopy on the surface of bulk solids.[42] In the latter case, the implementation of off-site excitation scheme in STM-based atomic-scale optical spectroscopy may be preferable. The off-site excitation scheme may also be advantageous to enhance sensitivity in elastic near-field scattering, which can suffer from interference with the background from far-field.[42] In addition, efficient off-site excitation of the LSP in STM could be advantageous for ultrafast STM to reduce background photoemission currents and to enable the local optical excitation of the sample without large-scale sample illumination.

To evaluate SPP nanofocusing in low-temperature STM, an *in-situ* evaluation method to quantitively compare the field enhancement generated by off-site versus tip-apex excitation of

LSPs within the STM junction is needed. Two experimental approaches are available for this purpose: (1) detection of elastically or inelastically scattered light; (2) measuring photo-induced tunneling currents. Inelastic light scattering, such as tip-enhanced Raman spectroscopy, is often employed to evaluate the near-field intensity within STM junctions.[16,43] In addition, photoemission current excited by femtosecond laser from free-standing nanotips[44,45] or STM tips[37,46] allows to evaluate the near-field intensity achieved by SPP nanofocusing.

Here, we introduce an additional approach for evaluating the field enhancement in plasmonic STM junctions using plasmon-assisted field emission resonances (FERs).[47] This method offers a practical and reliable approach for *in-situ* characterization of the near-field intensity during STM operation. Specifically, we demonstrate that it allows quantifying the relative field enhancement of direct tip-apex illumination versus off-site excitation of the LSP inside an Au-tip – Ag(111)-substrate junction. The intensity of the plasmon-assisted FERs, which are probed by highly localized tunneling current,[47] serve as a sensitive probe for the near-field intensity inside the STM junction. Compared to photoemission currents,[37,44-46] plasmon-assisted FERs are generated by one-photon absorption, i.e., a linear process, making it more accessible within the intensity range available in tip-enhanced Raman and photoluminescence spectroscopy.[48] In contrast to previous studies which employed a grating coupler for off-site excitation and comparison of the resulting field enhancement with direct apex illumination,[16,44] our work uses a single-groove coupler. This is a simplified version of a grating for very small laser spot sizes comparable to the groove size and has been employed to generate white "nanolight".[21] However, a direct comparison of the near-field enhancement achieved by a single-groove coupler with that of direct tip-apex illumination has not been carefully investigated.

2. Methods

Grooved tip design: Prior to tip fabrication, we conducted numerical simulations to examine the geometric parameters of the groove and pyramid shape of the tip shaft, aiming to maximize near-field enhancement at the tip apex under groove illumination (details in Supplementary Section 1). **Fig. 2(a–c)** illustrate the tip geometry, indicating five adjustable parameters: the distance between the groove edge and the tip apex (L), the width (W) and depth (D) of the groove, and the apex angles (θ_1 and θ_2). The value L of 10 μm ensures sufficient separation between the apex and the groove compared to the focal spot size of approximately 4 μm while minimizing damping of the SPP during propagation from the groove to the apex.[14,49] By evaluating the field enhancement across different parameters, we obtain W=900 nm, D=300 nm, θ_1=10° and θ_2=20° as a nearly optimal combination. We chose the near optimal because we traded some field enhancement for easier fabrication. **Fig. 2d** shows an SEM of the tip fabricated by focused ion beam milling. The designed tip shape is perfectly reproduced. More Details about the tip design, simulation, and fabrication are described in the Supplementary Section 1.

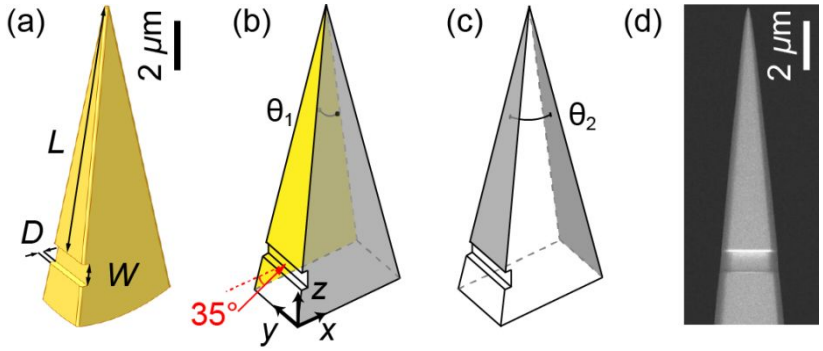

Fig. 2 Design and fabrication of the grooved pyramid tip. (a-c) Structural parameters of the grooved pyramid tip; The red arrow indicates the central axis of the incident Gaussian beam. (d) SEM image of the fabricated tip.

Experimental: The experiments were performed in a UHV chamber (base pressure $<5\times10^{-10}$ mbar) equipped with a low-temperature STM (modified UNISOKU USM-1400). The STM bias voltage (V) is applied to the Ag(111) sample and the tip is grounded. The Ag(111) surface was cleaned by repeated cycles of Ar^+ sputtering and annealing up to 670 K, yielding an

atomically flat surface. The UHV chamber has fused silica windows for optical access. A CW laser (633 nm or 780 nm) is focused on the STM junction at an angle of 55° with respect to the tip central axis using an *in-situ* Ag-coated parabolic mirror mounted on the cryogenic STM stage. The diameter of the incident beam is around 5 mm, and the focus of the parabolic mirror is 8.85 mm. Accurate beam alignment and focusing is achieved by piezo motors (Attocube GmbH) to position the parabolic mirror and to align three translational and two rotational axes. The laser is polarized along the plane spanned by the tip axis and the axis of the laser beam, and the diameter of the focal spot is estimated to be 6λ (where λ is the laser wavelength), which is estimated by scanning the focal spot across the tip apex and recording the distance over which the tip apex lights up. The movement of the parabolic mirror (and hence the laser spot) is calibrated from the known distance between the apex and the groove and the scattered light we observe from the junction (inset in **Fig. 1**).

Turning the laser on or off causes thermal expansion of the tip, disturbing the measurements. To eliminate its impact, all measurements started several minutes after starting or stopping laser illumination, when thermal expansion is no longer detectable. The thermal expansion is monitored by measuring the tip height, i.e., change in the piezoelectric tube length, while maintaining a constant gap distance through the feedback loop. The differential conductance ($\partial j/\partial V$) spectra are recorded using a lock-in amplifier with 20 mV modulation at a frequency of 983 Hz. All measurements are conducted at 15 K.

3. Results and discussion

The insets in **Fig. 1** display optical images of light scattered from the groove and the tip-apex. As the laser focal spot is scanned along the tip axis, we observe two intensity maxima in the back-scattered light when the laser spot is at the apex and the groove, respectively. These

maxima serve as indicators for precise positioning of the laser spot on the groove or the apex. In **Fig. 1b**, light scattering is observed from the groove when the tip apex is directly illuminated, indicating that SPPs propagate along the tip shaft and couple to the far-field at the groove. Conversely, the opposite behavior is expected when focusing the laser on the groove. However, strong back-reflection from the groove makes it challenging to observe the scattered light from the apex due to the limited dynamic range of the camera.

Fig. 3a shows $\partial j/\partial V$ spectra measured under dark conditions (gray) and during 780-nm laser illumination, for the laser being focused on the tip apex (blue curve) and the groove (red curve). In the constant-current mode (CCM) without illumination, we observed the first FER peak at 4.1 V, which corresponds to the image potential state on the Ag(111) surface.[50] Off-site excitation with a 780-nm laser induces a shift in the first FER peak from its original position at V_1=4.1 V to V_1'=2.6 V, resulting in a difference of $|\Delta V_1|$=1.5 V, where $\Delta V_1 = V_1' - V_1$ and V_1 and V_1' represent the position of the first FER peak before and during laser illumination, respectively. The peak shift $|\Delta V_1|$=1.5 V under off-site excitation is approximately equals to the incident photon energy of 1.59 eV. When the tip apex is illuminated directly, the first plasmon-assisted FER peak appears at V_1'=2.9 V, corresponding to a difference of $|\Delta V_1|$= 1.2 V relative to the original peak at V_1=4.1 V, such that the $|\Delta V_1|$ is smaller than the incident photon energy. The plasmon-assisted first FER peak arises from a resonant electron tunneling process in which an electron tunneling from the tip gains energy by absorption of a photon, such that it can tunnel into the image potential state at lower bias voltage.[47] The different $|\Delta V_1|$ between off-site and tip-apex illumination is attributed to an energetic shift of the image potential state due to different gap distances as explained in the Supplementary **Fig. S3a**. Most importantly, we find that the plasmon-assisted first FER peak is stronger under off-site excitation than that under apex illumination, indicating that the near-field intensity is higher than that achieved with direct tip-apex illumination.

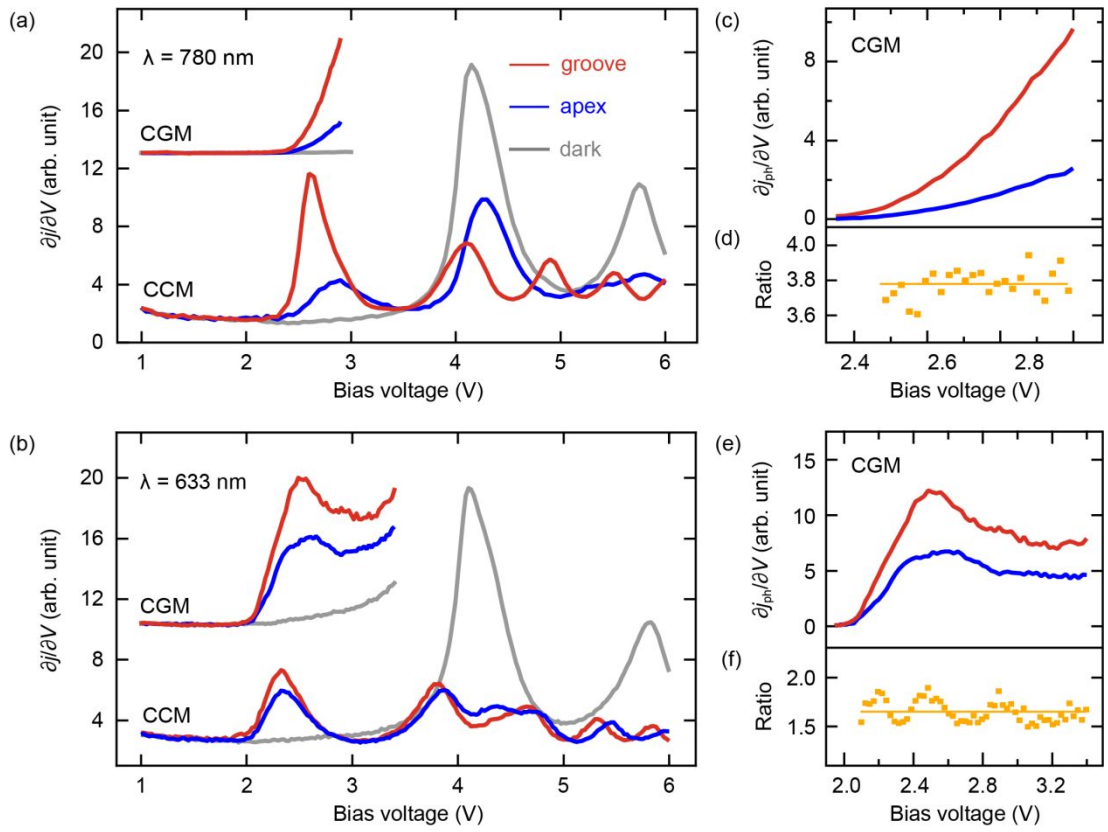

Fig. 3. (a, b). $\partial j/\partial V$ spectra acquired on Ag (111) surface under apex (blue) or groove (red) illumination showing FER peaks. The excitation wavelengths are 780 nm (hν= 1.59 eV) and 633 nm (hν= 1.96 eV), with the laser intensities at the focus are 9.6 kW/cm^2 and 8.8 kW/cm^2, respectively. The grey curves represent the spectrum without illumination. The constant current mode (CCM) spectra were acquired with a current setpoint of 0.1 nA. The constant-gap-distance mode (CGM) spectra are acquired with the gap distance set by a tunneling current of 0.1 nA at 1 V. The CGM spectra are shifted vertically for clarity. (c, e) $\partial j_{\mathrm{ph}}/\partial V$ spectra acquired at constant gap distance set by a tunneling current of 0.1 nA at 1 V. (d, f) the ratios (orange dots) of $\partial j_{\mathrm{ph}}/\partial V$ under groove to those under apex illumination. The solid lines indicate the average value.

In CCM, the gap distance varies with bias voltage as well as different near-field intensity caused by off-site and tip-apex excitation (supplementary **Fig. S3**), as different bias voltage or near-field intensity result in different photocurrent assuming that the gap distance is constant. To ensure a fair comparison of the near-field intensities between the two excitation schemes, it is essential to measure and compare the FER spectra in constant gap-distance mode (CGM) and to maintain the same gap distance across different excitation configurations or across varying illuminating power. We employ the same STM setpoint for all FER measurements

(e.g., V = 1 V and I = 0.1 nA) and verify that photocurrents are negligible at this setpoint, ensuring that the gap distance is determined by the static current after thermal equilibration of the electrons in metals (see Supplementary **Fig. S4** for details). The $\partial j/\partial V$ spectra in **Fig. 3a** recorded in CGM show a slope with an onset at V~2.4 V during off-site and tip-apex excitation. The signal is again significantly higher under off-site excitation.

The data in **Fig. 3b** is measured at an excitation wavelength of 633 nm. In the CCM spectra, illumination causes a shift of the first FER peak by $|\Delta V_1|$=1.8 V to V_1'=2.3 V, with $|\Delta V_1|$ closely matching the photon energy of 1.96 eV. In the CGM spectra, the plasmon-assisted FER peaks appear at a slightly higher voltage of V_1'=2.5 V, which we attribute to the energy shift of the image potential state caused by differences in gap distances between the CCM and CGM (Supplementary **Fig. S3b** for details).

To quantitatively compare the near-field intensities of the LSPs excited by tip-apex and off-site excitation, the current in CGM can be expressed as

$$j(V,|E_{\mathrm{A}}|) = j_{\mathrm{d}}(V) + j_{\mathrm{ph}}(V,|E_{\mathrm{A}}|) = j_{\mathrm{d}}(V) + c_1 f_1(V)|E_{\mathrm{A}}|^2 \quad (1)$$

where j is the total current under illumination, j_{d} is dark current, E_{A} is the electric field of the LSP at the apex and j_{ph} is photocurrent. Assuming that V and the local field E_{A} affect the j_{ph} independently, the one-photon photocurrent can be written as a product of a bias-dependent function $f_1(V)$ and the square amplitude of the local electric field ($|E_{\mathrm{A}}|^2$). The laser intensity dependence of the photocurrent in the Supplementary **Fig. S5** verifies that the first plasmon-assisted FER peak originates from a one-photon process. By taking the derivative of Eq (1), we obtain

$$\frac{\partial j_{\mathrm{ph}}(V,|E_{\mathrm{A}}|)}{\partial V} = \frac{\partial j(V,|E_{\mathrm{A}}|)}{\partial V} - \frac{dj_{\mathrm{d}}(V)}{dV} = c_1 f'_1(V)|E_{\mathrm{A}}|^2 \quad (2)$$

Therefore, $\frac{\partial j_{\mathrm{ph}}(V,|E_{\mathrm{A}}|)}{\partial V}$ can be determined from the spectra in **Fig. 3(a,b)** recorded in CGM, which give $\frac{\partial j}{\partial V}$ and $\frac{dj_{\mathrm{d}}}{dV}$ for the illuminated and dark case, respectively. $\frac{\partial j_{\mathrm{ph}}}{\partial V}$ is plotted in **Fig.**

3(c,e). Denoting $|E_A|$ under groove and apex illumination as $|E_A^{iG}|$ and $|E_A^{iA}|$, respectively, we derive at the following relationship:

$$\frac{\partial j_{ph}(V,|E_A^{iG}|)}{\partial V}\Big/\frac{\partial j_{ph}(V,|E_A^{iA}|)}{\partial V}=\frac{|E_A^{iG}|^2}{|E_A^{iA}|^2} \quad (3)$$

This shows that the ratio of $\frac{\partial j_{ph}}{\partial V}$ measured under groove and tip-apex excitation equals the ratio of the local intensities, $\frac{|E_A^{iG}|^2}{|E_A^{iA}|^2}$, and is independent of the bias voltage. **Fig. 3(d,f)** display the ratios plotted versus the bias voltage. The average ratio is indicated by the horizontal line. The data points are distributed randomly on both sides of the line, indicating that the ratio is indeed independent on the bias voltage, validating the relationship in Eq (3). We find that the average near-field intensity ratio is $\frac{|E_A^{iG}|^2}{|E_A^{iA}|^2}\approx 3.8$ for the excitation wavelength of 780 nm and 1.7 for 633 nm. We also note that the oscillatory behavior of the ratio in **Fig. 3f** is due to noise from the lock-in amplifier (Supplementary **Fig. S6**) and does not have any physical meaning.

The fact that the measured intensity ratio is greater than unity indicates that the energy flux directed into the LSP through off-site excitation surpasses that achieved by direct tip-apex excitation. The energy flux (SI unit: $J{\cdot}s^{-1}$) refers to the rate of energy transfer through a surface (not per unit area). In the groove-coupled off-site excitation, a fraction of far-field energy flux is initially converted into propagating SPPs. During the nanofocusing process, the SPPs are damped by ohmic loss and radiating into the far-field, and some remaining energy is converted into LSPs creating a localized field inside the STM junction. The far- to near-field conversion efficiency is defined as the fraction of total incident energy flux that is directed into the near-field region inside the STM junction. Since the size of the near-field is the same under both excitation scheme, the ratio of conversion efficiency for off-site versus tip-apex excitation equals the ratio of the near-field intensity.[16] The larger conversion efficiency observed for off-site excitation can be attributed to the larger geometric cross-section of the groove, fitting the

size of laser focal spot better, and compensates for the additional SPP loss. Last, it worths mention that the intensity ratio of 3.8 at the excitation wavelength of 780 nm in this study is only slightly lower than the reported intensity ratio of 4.4 achieved for gratings at 785-nm wavelength.[16#]

To further demonstrate the sensitivity of the intensity of the FER peak to the change of the near-field intensity, we examine the variation of plasmon-induced $\partial j_{\mathrm{ph}}/\partial V$ signal as the laser focal spot is scanned along the tip axis (**Fig. 4a**). **Fig. 4b** displays the constant-gap-distance $\partial j/\partial V$ spectra obtained at various focal positions along the tip. The first plasmon-assisted FER peak at V=2.5 V appears when the laser is focused on either the groove or the apex. **Fig. 4c** shows the resulting photocurrent and $\partial j_{\mathrm{ph}}/\partial V (= \partial j/\partial V - \partial j_d/\partial V)$ at 2.5 V as a function of the focus position. The $\partial j_{\mathrm{ph}}/\partial V$ spectra exhibit features of plasmon-assisted FER when the laser is focused on either the groove or the apex, but these features are absent when the focal spot is positioned between them. The plasmon-induced $\partial j_{\mathrm{ph}}/\partial V$, which directly reflects the near-field intensity in the junction, is sensitive to a change of the laser focus position

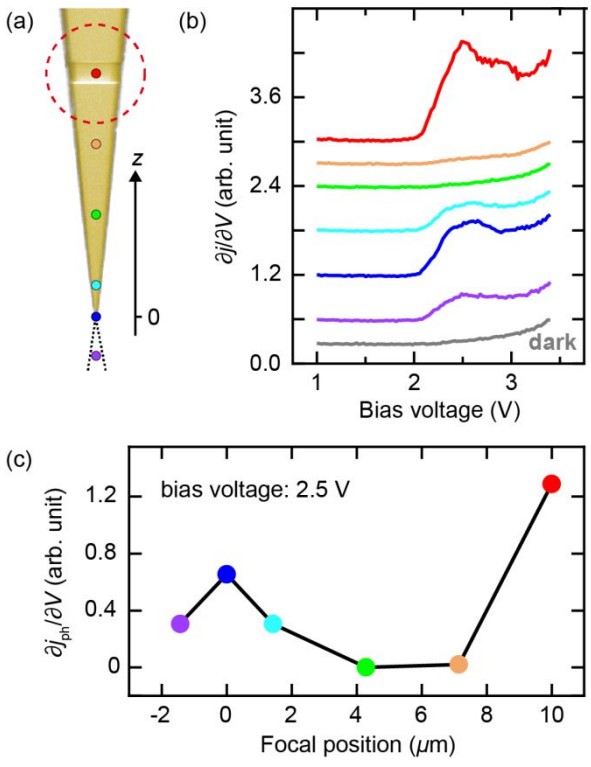

Fig. 4. (a) Laser-spot positions for spectra acquisition along the tip axis. A SEM image of the tip is used for illustration purpose. The dashed circle illustrates the size of the focused beam. The purple dot means the laser spot at the mirror image of the tip (dashed outline). (b) $\partial j/\partial V$ spectra obtained at the focal positions marked in (a) with a 633-nm excitation wavelength. The spectra were recorded in the constant gap-distance mode at a gap distance set by V=1 V and j=0.1 nA. (c) $\partial j_{\mathrm{ph}}/\partial V$ at V=2.5 V as a function of focal position.

of approximately 1 μm. This sensitivity suggests that the plasmon-assisted FER peak serves as a reliable indicator for precise optimization of the beam position on the tip.

To obtain further insights into the differences between the groove and apex illumination, we simulated the distributions of electric-field enhancement for both configurations. **Fig. 5** presents the results for an excitation wavelength of 780 nm. The electric-field enhancement factor under groove (apex) illumination is defined as $\left|E_{\mathrm{A}}^{\mathrm{iG(A)}}\right|/|E_{\mathrm{laser}}|$, where $|E_{\mathrm{laser}}|$ denote the electric-field amplitude of the incident laser at the center of the focal spot. Since $|E_{\mathrm{laser}}|$ is identical for both groove and apex illumination, the ratio of field enhancement factors is equivalent to the ratio of the electric-field amplitudes $\frac{|E_{\mathrm{A}}^{\mathrm{iG}}|}{|E_{\mathrm{A}}^{\mathrm{iA}}|}$. **Fig. 5(a–b)** compare the spatial distribution of the field enhancement along the surface of the pyramid tip. In the case of off-site excitation, a small fraction of the nanofocused SPPs reflects back from the apex and interferes with the counter-propagating SPPs along the shaft, forming weak interference fringes.

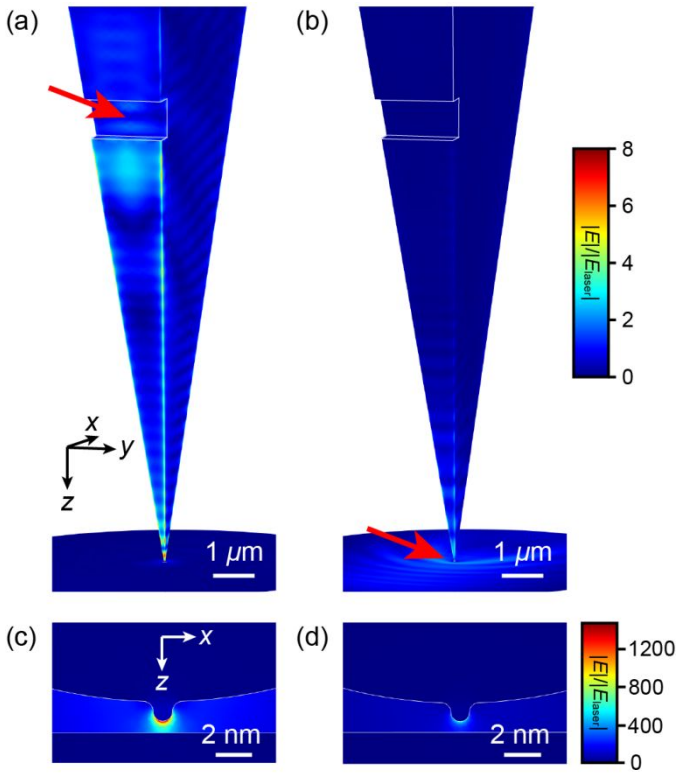

Fig. 5. Distributions of the enhancement factor under groove (a,c) and apex (b,d) illumination at an excitation wavelength of 780 nm. The incident wave vector (red arrow) is in the x–z plane and forms an angle of 35° with respect to the horizontal plane.

In contrast, only weak SPP intensity and interference effects are observed for direct illumination of the tip apex, because the SPPs diverge, and their intensity decreases during propagating towards the groove. **Fig. 5(c–d)** show that the maximum field enhancement occurs at the atomic-scale protrusion under both groove and apex illumination. However, the field enhancement at the atomic-scale protrusion is significantly higher under groove illumination compared to apex illumination, further supporting the superior efficiency of groove-coupled off-site excitation in concentrating the field enhancement at the junction.

Table 1 lists the field enhancement factors at the very apex of the tip under both off-site and tip-apex excitation . These values quantify the amplification of the electric field at the apex with the respective excitation schemes. The field enhancement factors reach several hundred within the gap formed between the tip and the Ag surface and are further amplified by approximately five-fold with the addition of an atomic-scale protrusion (picocavity) with both excitation schemes. At an excitation wavelength of 780 nm, the ratio of the near-field intensity under off-site excitation to that under tip-apex excitation is approximately 6.6, irrespective of the presence of the atomic-scale protrusion. This confirms that the efficiency of groove-coupled off-site excitation of the LSP significantly surpasses that of direct tip-apex illumination. We note that the simulated intensity ratio represents an upper limit, as it assumes a perfectly smooth pyramid surface with minimal SPP scattering losses due to surface roughness during the nanofocusing process. The experimental value of 3.8 corresponds to 57% of the theoretical value. At the excitation wavelength of 633 nm, the simulated ratio of the near-field intensity for off-site versus tip-apex excitation decreases to approximately 4.6. The smaller value than that obtained for 780 nm is attributed to higher damping and ohmic loss for SPPs at higher frequencies.[49] The experimental ratio is approximately 1.7, corresponding to approximately 39% of the theoretical value predicted by the simulation. This discrepancy likely arises from imperfect surface conditions and additional energy dissipation experienced by the SPPs in the

experiments.

Table 1. Field enhancement factors at the tip apex under groove and apex illumination, along with the ratios of near-field intensities.

λ (nm)	$\|E_A^{iG}\|/\|E_{Laser}\|$	$\|E_A^{iA}\|/\|E_{Laser}\|$	$\|E_A^{iG}\|^2/\|E_A^{iA}\|^2$	$\|E_A^{iG}\|^2/\|E_A^{iA}\|^2$
	simulation	simulation	simulation	experiment
633	1218 (239)	568 (108)	4.6 (4.9)	1.7
780	1426 (383)	556 (148)	6.6 (6.7)	3.8

The values without parentheses are for structures with atomic-scale protrusions at the apexes, while the values in parentheses are for structures without protrusions.

To further validate the approach and underlying principles of our analysis, we analyze the dependence of the field enhancement at the tip apex on the geometric parameters of the grooved tip and outline the process of determining the optimal parameters for the tip shape using numerical simulations. **Fig. 6(a–d)** shows two-dimensional plots of the electric-field enhancement $|E_A|/|E_{laser}|$, where $|E_A|$ is the electric-field amplitude at the tip apex and $|E_{laser}|$ is the electric-field amplitude in the center of the laser focus. **Fig. 6(a,b)** explore various combinations of groove widths (W) ranging from 100 nm to 1000 nm and depths (D) ranging from 100 nm to 500 nm at the excitation wavelengths of 780 nm and 633 nm, respectively. The groove distance (L=10 μm) and apex angles (θ_1=10° and θ_2=20°) are kept constant. The simulation results are in general agreement with a previous theoretical study on SPP excitation with a single groove,[51] validating the approach and underlying principles of our analysis. At the excitation wavelength of 780 nm, the highest enhancement factors of 19.3 and 19.0 are obtained at W=800 nm, D=300 nm and W=900 nm, D=300 nm, respectively. At the excitation wavelength of 633 nm, the best enhancement factors of 8.1, 8.0, and 7.8 occur at W=1000 nm, D=200 nm, W=1000 nm, D=300 nm and W=900 nm, D=300 nm, respectively. Therefore, the combination of W=900 nm and D=300 nm is selected as it gives one of the best enhancements at both wavelengths.

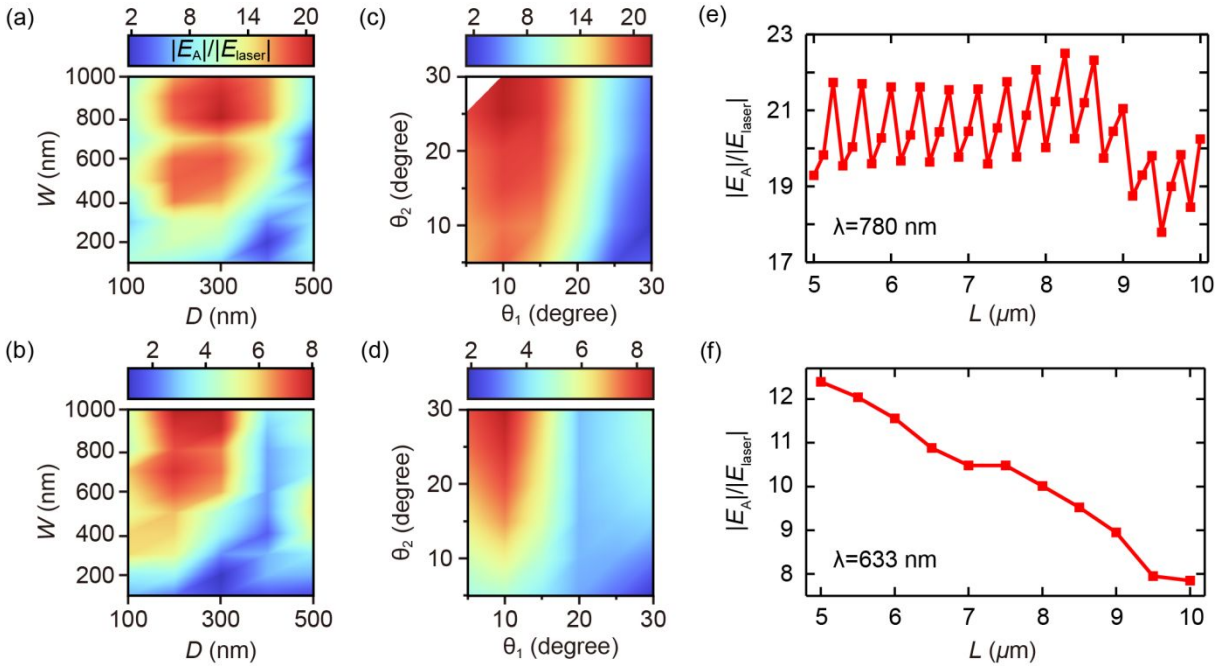

Fig. 6 Enhancement factor of electric field at the tip apex as a function of (a,b) groove width *W* and depth *D*, (c,d) apex angles θ_1 and θ_2, and (e,f) groove-to-apex distance *L*. Fixed parameters: (a,b)θ_1=10°, θ_2=20°, and L=10 μm. (c,d) *W*=900 nm, *D*=300 nm, and L=10 μm. (e,f) θ_1=10°, θ_2=20°, *W*=900 nm, and *D*=300 nm. The excitation wavelength is 780 nm in (a,c,e) and 633 nm in (b,d,f).

Next, the apex angles are optimized with fixed values of *W*=900 nm and *D*=300 nm. In general, the angle θ_1 has a greater influence on the enhancement factor than θ_2, as shown in **Fig. 6(c,d)**. Decreasing θ_1 enhances the nanofocusing effect,[52] however, it also reduces groove length, which in turn reduces the laser radiation received by the groove. At θ_1=25°, the groove length becomes comparable to the diameter of the focused beam. Initially, as θ_1 decreases, the enhancement factor increases because the enhanced adiabatic nanofocusing dominates. However, when θ_1 drops below 10°, the reduction in the laser radiation received by the groove becomes dominant, leading to a decrease in the enhancement factor. The maximum enhancement factors are achieved at θ_1=10°, θ_2=25° and θ_1=10°, θ_2=30° for the excitation wavelengths of 780 nm and 633 nm, respectively. We select θ_1=10° and θ_2=20° because this combination is easier to fabricate due to a smaller difference between θ_1 and θ_2. The enhancement factor at θ_1=10° and θ_2=20° corresponds to approximately 90% of the maximum

enhancement factor at both excitation wavelengths. In conclusion, we obtain W=900 nm, D=300 nm, θ_1=10° and θ_2=20° as a near-optimal combination.

As discussed above, the groove–apex distance (L) is fixed at 10 μm. Subsequently, we investigate the the influence of L on the field enhancement at the tip apex, as shown in **Fig. 6(e,f)**. At the excitation wavelength of 780nm, the field enhancement oscillates with a periodicity of approximately λ/2 as L varies from 5 μm to 10 μm. This is attributed to the interference within the Fabry-Pérot cavity formed between the groove and the tip apex. Notably, the peak values of the oscillations remains nearly constant as L varies from 5 μm to 9 μm. In contrast, at the excitation wavelength of 633 nm, the field enhancement decays significantly as L varies from 5 μm to 10 μm. The observed difference between the two wavelengths arises from the different SPP decay lengths (L_{SPP}). At 780 nm, the L_{SPP} is substantially longer than L,[53] allowing the increasing groove length in the y-direction (**Fig. 2**) to compensate for SPP loss by capturing more radiation. Conversely, at 633 nm, L_{SPP} is comparable to L,[53] resulting in SPP loss dominating the enhancement. Therefore, the performance of the grooved tip can be further improved by reducing L.

4. Conclusions

In summary, we developed a novel method for comparing near-field intensity under different excitation schemes in an STM junction using plasmon-assisted FERs. We applied this approach to evaluate the field enhancement of a plasmonic picocavity in a low-temperature STM, resulting from an off-site excitation via plasmonic nanofocusing. We fabricated a grooved pyramid tip with optimized geometric parameters that are W=900 nm, D=300 nm, θ_1=10° and θ_2=20° and quantified ratio of near-field intensity at the tip apex under off-site excitation relative to that under direct tip-apex excitation. At an excitation wavelength of 780

nm, the ratio of the near-field intensities under groove and apex illumination is close to 3.8, reaching 57% of the theoretical value. At the excitation wavelength of 633 nm, the ratio is 1.7, which corresponds to 38% of the theoretical value but is still greater than unity. These suggest that the grooved pyramidal tip is suitable for multi-wavelength excitations. Prospectively, the grooved pyramidal tip offers a relatively simple structure for tip-enhanced optical spectroscopy by effectively suppressing the significant far-field contributions, paving the way for more precise and background-free near-field spectroscopic studies.

Author contributions

Chenfang Lin: Investigation; Methodology (equal); Formal analysis (equal); Supervision (equal); Writing – review & editing (equal).

Jie Li: Formal analysis (equal); Writing – original draft (equal).

Guoao Li: Methodology (equal).

Wenjie Luo: Writing – original draft (equal).

Shuyi Liu: Resources (equal).

Adnan Hammud: Resources (equal).

Yang Xia: Resources (equal).

Anlian Pan: Resources (equal).

Martin Wolf: Resources (equal).

Melanie Müller: Writing – review & editing (auxiliary); Supervision (equal).

Takashi Kumagai: Conceptualization; Funding acquisition; Supervision (equal); Writing – review & editing (equal).

Data availability

Data for this article are available at Zenodo at https://doi.org/10.5281/zenodo.14600345

Conflicts of interest

There are no conflicts to declare.

Acknowledgements

The authors thank Hiroko Yoshino for supporting the experiments. T.K. acknowledges a support by JST FOREST Program (Grant Number JPMJFR201J, Japan). C.L. acknowledges the support by the Ministry of Science and Technology of the People's Republic of China (No. 2022YFA1204700), the National Natural Science Foundation of China (No. 12104146), the Natural Science Foundation of Hunan Province (No. 2022JJ20002), and the Fundamental Research Funds for the Central Universities (Nos. 227202101005, 227202201293).

Supplementary information

Electronic supplementary information (ESI) available. See DOI: https://doi.org/

Notes

[#] The TERS intensity is proportional to the fourth power of the electric-field amplitude, so we determined the near-field intensity ratio between grating and apex illumination to be approximately 4.4 after taking the square root of the ratio of TERS intensities, which is approximately 20 in the reference.

References

1. R. Gutzler, M. Garg, C. R. Ast, K. Kuhnke and K. Kern, *Nature Reviews Physics*, 2021, **3**, 441-453.
2. R. Zhang, Y. Zhang, Z. C. Dong, S. Jiang, C. Zhang, L. G. Chen, L. Zhang, Y. Liao, J. Aizpurua, Y. Luo, J. L. Yang and J. G. Hou, *Nature*, 2013, **498**, 82-86.
3. J. Lee, K. T. Crampton, N. Tallarida and V. A. Apkarian, *Nature*, 2019, **568**, 78-82.
4. B. Yang, G. Chen, A. Ghafoor, Y. Zhang, Y. Zhang, Y. Zhang, Y. Luo, J. Yang, V. Sandoghdar, J. Aizpurua, Z. Dong and J. G. Hou, *Nature Photonics*, 2020, **14**, 693-699.
5. M. Imai-Imada, H. Imada, K. Miwa, Y. Tanaka, K. Kimura, I. Zoh, R. B. Jaculbia, H. Yoshino, A. Muranaka, M. Uchiyama and Y. Kim, *Nature*, 2022, **603**, 829-834.
6. J. Y. Xu, X. Zhu, S. J. Tan, Y. Zhang, B. Li, Y. Z. Tian, H. Shan, X. F. Cui, A. D. Zhao, Z. C. Dong, J. L. Yang, Y. Luo, B. Wang and J. G. Hou, *Science*, 2021, **371**, 818-822.
7. Y. Park, I. Hamada, A. Hammud, T. Kumagai, M. Wolf and A. Shiotari, *Nat Commun*, 2024, **15**, 6709.
8. Q. Meng, J. Zhang, Y. Zhang, W. Chu, W. Mao, Y. Zhang, J. Yang, Y. Luo, Z. Dong and J. G. Hou, *Sci Adv*, 2024, **10**, eadl1015.
9. B. Cirera, M. Wolf and T. Kumagai, *ACS Nano*, 2022, **16**, 16443-16451.
10. F. Benz, M. K. Schmidt, A. Dreismann, R. Chikkaraddy, Y. Zhang, A. Demetriadou, C. Carnegie, H. Ohadi, B. de Nijs, R. Esteban, J. Aizpurua and J. J. Baumberg, *Science*, 2016, **354**, 726-729.

11. J. J. Baumberg, *Nano Lett.*, 2022, **22**, 5859-5865.
12. M. Urbieta, M. Barbry, Y. Zhang, P. Koval, D. Sanchez-Portal, N. Zabala and J. Aizpurua, *ACS Nano*, 2018, **12**, 585-595.
13. T. L. Vasconcelos, B. S. Archanjo, B. Fragneaud, B. S. Oliveira, J. Riikonen, C. Li, D. S. Ribeiro, C. Rabelo, W. N. Rodrigues, A. Jorio, C. A. Achete and L. G. Cancado, *ACS Nano*, 2015, **9**, 6297-6304.
14. H. Bockmann, M. Muller, A. Hammud, M. G. Willinger, M. Pszona, J. Waluk, M. Wolf and T. Kumagai, *J Phys Chem Lett*, 2019, **10**, 2068-2074.
15. F. Lu, W. Zhang, M. Liu, L. Zhang and T. Mei, *IEEE Journal of Selected Topics in Quantum Electronics*, 2021, **27**, 1-12.
16. S. Berweger, J. M. Atkin, R. L. Olmon and M. B. Raschke, *The Journal of Physical Chemistry Letters*, 2010, **1**, 3427-3432.
17. A. J. Babadjanyan, N. L. Margaryan and K. V. Nerkararyan, *J. Appl. Phys.*, 2000, **87**, 3785-3788.
18. M. I. Stockman, *Phys. Rev. Lett.*, 2004, **93**, 137404.
19. C. Ropers, C. C. Neacsu, T. Elsaesser, M. Albrecht, M. B. Raschke and C. Lienau, *Nano Lett.*, 2007, **7**, 2784-2788.
20. S. Berweger, J. M. Atkin, R. L. Olmon and M. B. Raschke, *J Phys Chem Lett*, 2012, **3**, 945-952.
21. T. Umakoshi, M. Tanaka, Y. Saito and P. Verma, *Science Advances*, 2020, **6**, eaba4179.
22. C. C. Neacsu, S. Berweger, R. L. Olmon, L. V. Saraf, C. Ropers and M. B. Raschke, *Nano Lett.*, 2010, **10**, 592-596.
23. K. Zhang, S. I. Taniguchi and T. Tachizaki, *Opt. Lett.*, 2018, **43**, 5937-5940.
24. K. V. Nerkararyan, *Phys. Lett. A*, 1997, **237**, 103-105.
25. D. K. Gramotnev and S. I. Bozhevolnyi, *Nature Photonics*, 2013, **8**, 13-22.

26. M. Esmann and C. Lienau, *Microscopy and Analysis*, 2020, **47**, 22-23.

27. D. Xu, B. Liang, Y. Xu and M. Liu, *Nano Research*, 2022, **16**, 5555-5571.

28. A. Wöste, G. Hergert, T. Quenzel, M. Silies, D. Wang, P. Groß and C. Lienau, *Nano Lett.*, 2023, **23**, 5528-5534.

29. W. Luo, R. Song, B. G. Whetten, D. Huang, X. Cheng, A. Belyanin, T. Jiang and M. B. Raschke, *Small*, 2024, **20**, 2307345.

30. W. Luo, B. G. Whetten, V. Kravtsov, A. Singh, Y. Yang, D. Huang, X. Cheng, T. Jiang, A. Belyanin and M. B. Raschke, *Nano Lett.*, 2023, **23**, 1767-1773.

31. T. Jiang, V. Kravtsov, M. Tokman, A. Belyanin and M. B. Raschke, *Nature Nanotechnology*, 2019, **14**, 838-843.

32. T. Umakoshi, Y. Saito and P. Verma, *Nanoscale*, 2016, **8**, 5634-5640.

33. K. Tomita, Y. Kojima and F. Kannari, *Nano Lett.*, 2018, **18**, 1366-1372.

34. X. Ma, Y. Zhu, N. Yu, S. Kim, Q. Liu, L. Apontti, D. Xu, R. Yan and M. Liu, *Nano Lett.*, 2019, **19**, 100-107.

35. K. Zhang, Y. Bao, M. Cao, S.-I. Taniguchi, M. Watanabe, T. Kambayashi, T. Okamoto, M. Haraguchi, X. Wang, K. Kobayashi, H. Yamada, B. Ren and T. Tachizaki, *Anal. Chem.*, 2021, **93**, 7699-7706.

36. V. Kravtsov, R. Ulbricht, J. M. Atkin and M. B. Raschke, *Nat Nanotechnol*, 2016, **11**, 459-464.

37. G. A. Traeger, M. H. Teichmann, B. Schröder and M. Wenderoth, *Rev. Sci. Instrum.*, 2023, **94**, 023702.

38. B. Pettinger, P. Schambach, C. J. Villagomez and N. Scott, *Annu. Rev. Phys. Chem.*, 2012, **63**, 379-399.

39. A. Shiotari, T. Kumagai and M. Wolf, *The Journal of Physical Chemistry C*, 2014, **118**, 11806-11812.

40. H. An, J. Li, Y. Liu, P. Xu, S. Han, Y. Liu, S. Chen, S.-Y. Li, C. Lin and A. Pan, *The Journal of Physical Chemistry C*, 2024, **128**, 7583-7590.
41. K.-D. Park, O. Khatib, V. Kravtsov, G. Clark, X. Xu and M. B. Raschke, *Nano Lett.*, 2016, **16**, 2621-2627.
42. A. Shiotari, J. Nishida, A. Hammud, F. Schulz, M. Wolf, T. Kumagai and M. Müller, *arXiv preprint*, 2024, **arXiv:2410**, 18455.
43. S. Liu, F. P. Bonafe, H. Appel, A. Rubio, M. Wolf and T. Kumagai, *ACS Nano*, 2023, **17**, 10172-10180.
44. M. Müller, V. Kravtsov, A. Paarmann, M. B. Raschke and R. Ernstorfer, *ACS Photonics*, 2016, **3**, 611-619.
45. J. Vogelsang, J. Robin, B. J. Nagy, P. Dombi, D. Rosenkranz, M. Schiek, P. Gross and C. Lienau, *Nano Lett.*, 2015, **15**, 4685-4691.
46. B. Schröder, O. Bunjes, L. Wimmer, K. Kaiser, G. A. Traeger, T. Kotzott, C. Ropers and M. Wenderoth, *New Journal of Physics*, 2020, **22**, 033047.
47. S. Liu, M. Wolf and T. Kumagai, *Phys. Rev. Lett.*, 2018, **121**, 226802.
48. X.-B. Zhang, Y.-F. Zhang, H. Li, J. Cui, S. Jiang, B. Yang, Y. Zhang, Y. Zhang and Z.-C. Dong, *Chinese Journal of Chemical Physics*, 2022, **35**, 713-719.
49. H. Bockmann, S. Liu, M. Muller, A. Hammud, M. Wolf and T. Kumagai, *Nano Lett.*, 2019, **19**, 3597-3602.
50. T. Kumagai, S. Liu, A. Shiotari, D. Baugh, S. Shaikhutdinov and M. Wolf, *J Phys Condens Matter*, 2016, **28**, 494003.
51. J. Renger, S. Grafström and L. M. Eng, *Phys. Rev. B*, 2007, **76**, 045431.
52. R. Yadav, T. Umakoshi and P. Verma, *AIP Advances*, 2022, **12**, 085216.
53. M. Kuttge, E. J. R. Vesseur, J. Verhoeven, H. J. Lezec, H. A. Atwater and A. Polman, *Appl. Phys. Lett.*, 2008, **93**, 113110.

Data availability statements

Data for this article are available at Zenodo at https://doi.org/10.5281/zenodo.14600345